Chapter 2: Comparing and Contrasting the Mechanosenstive Channels of Large Conductance (MscL) from *E. coli* and *M. tuberculosis* and Verification of the *M. tuberculosis* Crystal Structure.

2.1 Introduction

Recent work has attempted to rationalize the extensive functional studies on *E. coli* MscL (Ec-MscL) in light of the crystal structure, which was obtained for the *M. tuberculosis* homologue (Tb-MscL) (Batiza et al., 1999; Blount and Moe, 1999; Chang et al., 1998; Oakley et al., 1999; Rees et al., 2000; Spencer et al., 1999). Additionally, several different models for channel opening have been proposed by considering *E. coli* gain of function (GOF) mutations in terms of the *M. tuberculosis* crystal structure (Batiza et al., 1999; Chang et al., 1998; Sukharev et al., 2001b). To critically evaluate these efforts, it is essential to assess the underlying assumption of the portability of Ec-MscL functional data to the Tb-MscL structure. While the function of the *E. coli* channel has been extensively probed by site-directed and random mutagenesis, analogous studies of the *M. tuberculosis* channel have not been reported (Batiza and Kung, 2000; Blount et al., 1998; Blount et al., 1997; Blount et al., 1996b; Liu et al., 1999; Ou et al., 1998; Yoshimura et al., 1999). Preliminary data have shown that wild-type *E. coli* and *M. tuberculosis* MscL are similar electrophysiologically. Both channels exhibit a large single channel conductance, approximately 3.5 nS, and gate with similar tensions in reconstituted liposomes (Moe et al., 2000; Shapovalov and Lester, 2000). However, the Tb-MscL channel exhibits twice the gating tension of Ec-MscL in *E. coli* spheroplasts (Moe et al., 2000). This difference may result from protein structural differences, a difference in interactions with lipids, or both.

Sequence alignment is essential to map previously studied *E. coli* GOF mutations onto the *M. tuberculosis* MscL sequence. In this work we report an optimal sequence

alignment of 35 MscL homologues and an information on regions of conservation and variability. Consistent with previous studies, we find greater conservation in the transmembrane regions than in the loop or intracellular regions. Interestingly, the various channels clearly fall into subfamilies based on sequence similarity, with Ec-MscL and Tb-MscL in different subfamilies.

Circular dichroism is a method of obtaining crude structural analysis of proteins and provides another estimate of overall similarity between homologous proteins. Here we present circular dichroism spectra of nine MscL homologues. As with the sequence analysis, MscL homologues fall into subfamilies based on their observed helicity. Surprisingly, the subfamilies obtained from circular dichroism analysis are different than those obtained from sequence analysis.

Using the optimal alignment, we have prepared Tb-MscL analogues of several critical Ec-MscL GOF mutations (Figure 2.1-A). Perhaps surprisingly, we find that several well-established Ec-MscL GOF mutants do not translate to the Tb-MscL system. We also directly evaluate a predicted intersubunit hydrogen bond in the Tb-MscL crystal structure (Figure 2.1-B). Cross-linking studies establish that these residues are indeed close in the reconstituted channel, and firmly establish the pentameric nature of the channel. Mutations of this pair generally lead to GOF mutants, suggesting an important functional role for this specific region of the channel. Interestingly, no analogous interaction is apparent in the Ec-MscL alignment. Our results indicate that the functional

studies performed on the Ec-MscL channel may not map directly onto the Tb-MscL crystal structure.

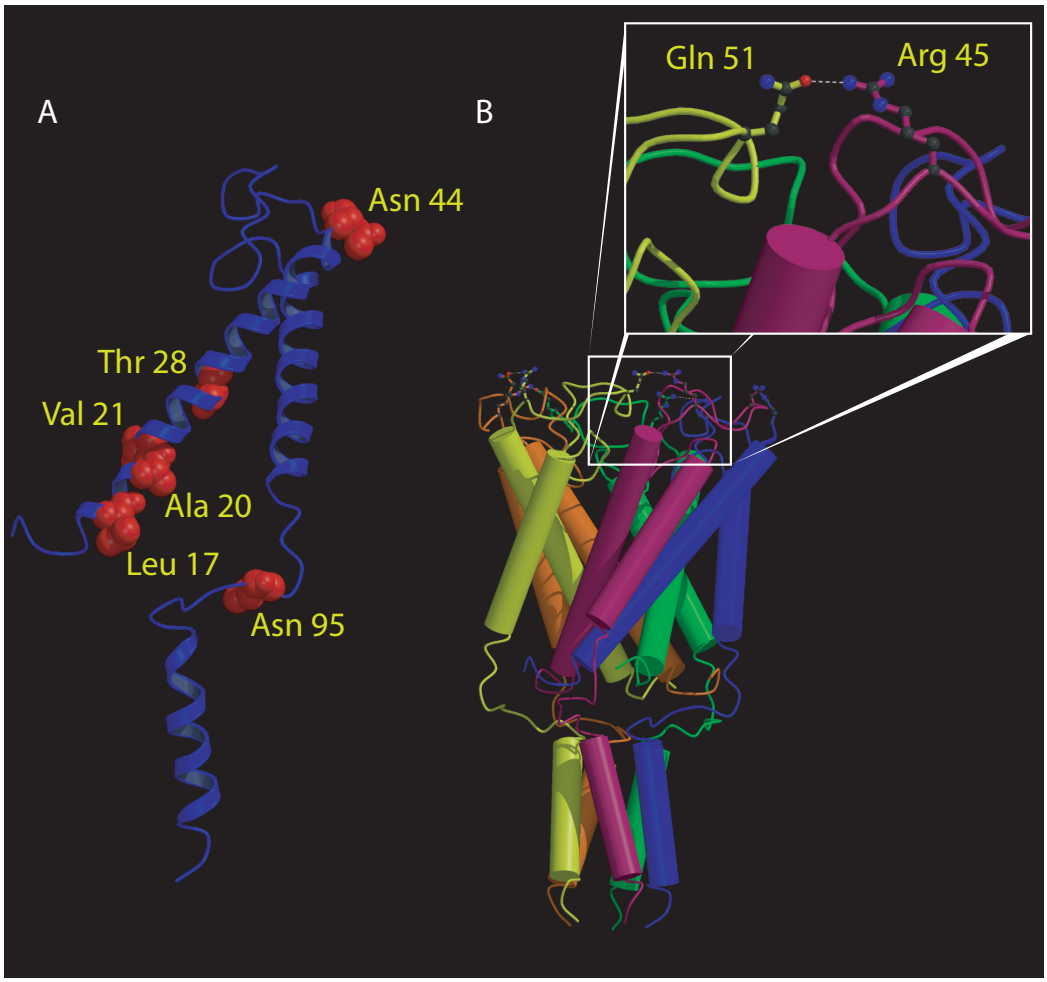

Figure 2.1: *M. tuberculosis* MscL crystal structure. **(A)** Severe and very severe GOF mutations from Ec-MscL are mapped onto one subunit of the Tb-MscL crystal structure. **(B)** The R45•••Q51 hydrogen bond. The box shows a closeup of the hydrogen bond between the yellow and purple subunits. Figures were generated with MOLSCRIPT and Raster3D.

2.2 Results

2.2.1 Sequence Analysis

Although clearly related, the mechanosensitive channels from various organisms show moderate to low sequence identities. For example, the sequence identity of Tb-MscL compared to Ec-MscL is 37%, while the sequence identity of *B. bronchiseptica* MscL compared to *M. leprae* MscL is 15%. Therefore, development of an optimal alignment is not straightforward. For this reason, we have augmented sequence alignment approaches with MEME analysis (Bailey and Elkan, 1994; Bailey and Gribskov, 1998), which identifies conserved regions within a group of sequences. Figure 2.2 shows an AMPS multiple sequence alignment and MEME group analysis of 35 putative MscL sequences. The MEME group analysis was used to make slight adjustments to the AMPS multiple sequence alignment using the indicated areas of conservation within the sequences. This alignment was further analyzed to determine which regions of MscL were most divergent using AMPS pairwise alignment of the full sequences and of selected regions, such as the first and second transmembrane domains, the extracellular loop, and the carboxy terminus. Regional divisions were made by applying the previous definitions from the Tb-MscL crystal structure to the multiple sequence alignment (Chang et al., 1998). These alignments indicate general overall similarity for all regions of the protein; however, the loop region clearly shows the most variability. Contour plots showing scores for the AMPS pairwise alignments of the first transmembrane domain, the extracellular loop, and the carboxy terminus are shown in Figure 2.3.

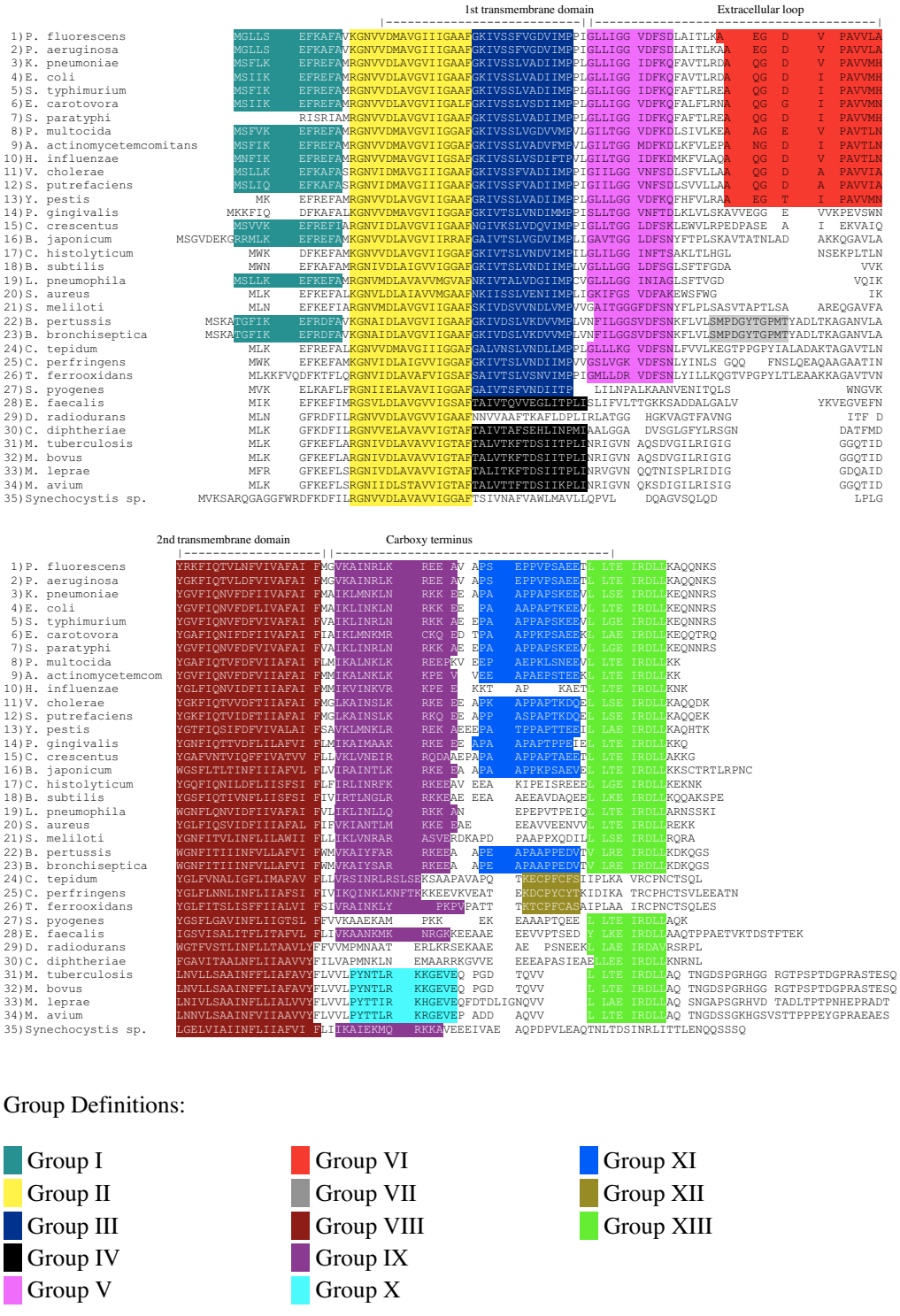

Figure 2.2: MEME consensus group analysis shown on the AMPS multiple sequence alignment. The AMPS multiple sequence alignment of 35 putative MscL sequences is shown. The colored regions on the sequence alignment indicate MEME consensus groups.

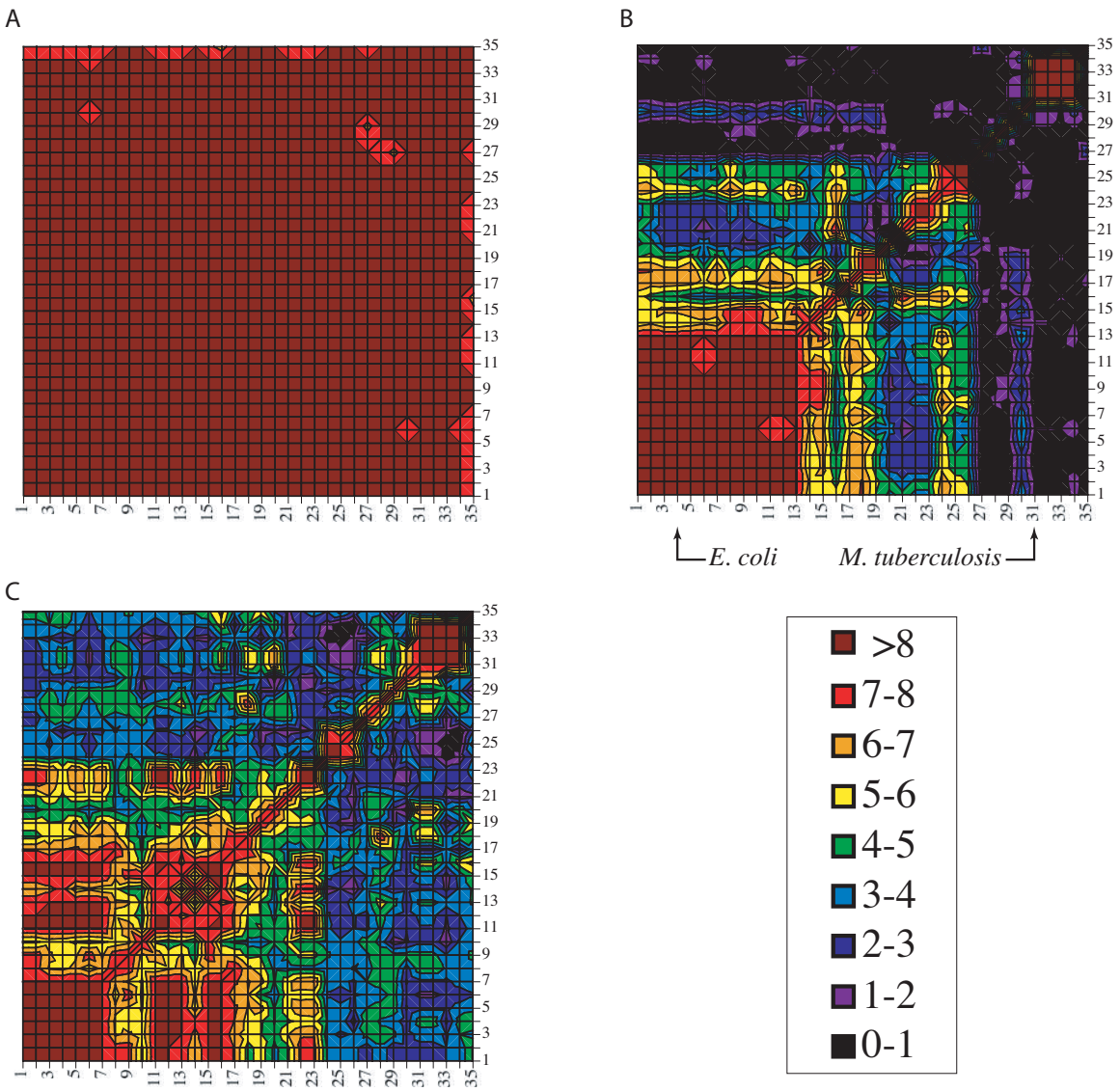

Figure 2.3: Regional AMPS pairwise alignments for the first transmembrane domain, the loop region, and the carboxyl terminus. Numbers on axes correspond to the sequence numbers in Figure 2. (A) The contour plot for the first transmembrane domain shows that this region of the MscL protein is almost completely conserved. (B) The loop region shows much more diversity than seen in the first transmembrane domain. Very low scores are observed for some pairs of proteins in this region. The contour plot shows groupings of sequences, with a large subfamily containing *E. coli* and a smaller subfamily containing *M. tuberculosis*. (C) The contour plot of the carboxyl terminal region shows more diversity than observed for the first transmembrane domain, however less diversity than observed for the loop region.

2.2.2 Comparative Circular Dichroism Studies

Circular dichroism was used to compare the subset of MscL homologues that have been functionally characterized (Moe et al., 1998). The spectra obtained for these homologues are shown in Figure 2.4, and selected features are listed in Table 2.1. As observed with the sequence alignment of MscL homologues, the homologues fall into two distinct families. The families resulting from the circular dichroism studies are different than those observed from the sequence alignment data. Based on the observed circular dichroism spectra, the first family is composed of *E. coli*, *H. influenza*, and *P. fluorescens* and the second family is composed of *M. tuberculosis*, *E. carotovora*, *C. perfringens*. *S. aureus*, *B. subtilis*, and *Synechocytis sp*.

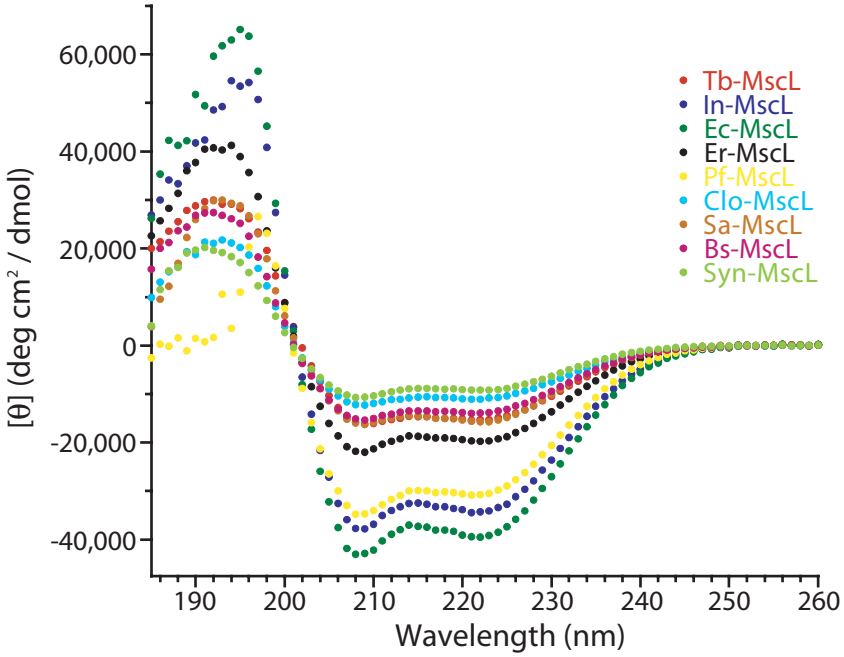

Figure 2.4: Circular dichrosims spectra for nine different homologues of the mechanosenitive channel of large conductance. Two groupings of channels are observed from the CD data with Ec-MscL and Tb-MscL lying in different groups.

Using the elipticity at 222 nm observed in the circular dichrosim spectra, the percent helicity of each MscL homologue was estimated as previously described for Ec-MscL (Brunger Method) (Arkin et al., 1998). Additionally, the percent helical content for each sequence was predicted using Jpred (Cuff and Barton, 1999). These data are shown in Table 2.1.

Species	Abbreviation	Sequence number	Helical Content from CD	Helical Content from Jpred
P. fluorescens	Pf	1	85-51%	48%
H. influenza	In	10	95-57%	56%
E. coli	Ec	4	110-66%	53%
E. carotovora	Er	6	55-33%	49%
M. tuberculosis	Tb	31	42-25%	45%
C. perfringens	Clo	25	31-18%	35%
S. aureus	Sa	20	44-26%	50%
B. subtilis	Bs	18	39-23%	52%
Synechocystis sp.	Syn	35	25-15%	50%

Table 2.1: A summary of the circular dichroism specra for various homologues of MscL. Jpred predictions of helical content are based on sequence analaysis. Helical content fro the various MscL homologues was determined from the abosorbance in the CD spectrum at 222 nm using the method previously described for Ec-MscL

Since MscL homologues vary considerably in length from 143 amino acids to 175 amino acids, the observed helicity as a function of protein length was examined. Figure 2.5 shows a plot of the maximal helicity predicted for each homologue as a function of homologue length. No correlation is observed between these quantities.

2.2.3 Mutational Mapping

With an optimal alignment in hand (Figure 2.2), we were able to map some of the very severe and severe mutations from Ec-MscL onto Tb-MscL (Oakley et al., 1999). The

most extensively probed type of mutation has been the so-called gain of function (GOF) mutation. This is observed in growth studies of *E. coli* expressing the mutant channel. It is assumed that a mutation that increases channel opening probability will, in effect, put a hole in the cell membrane, which is deleterious to growth. The screen thus identifies channels that have a higher open probability at ambient pressure, which is considered a gain of function. (Blount et al., 1997; Ou et al., 1998; Yoshimura et al., 1999)

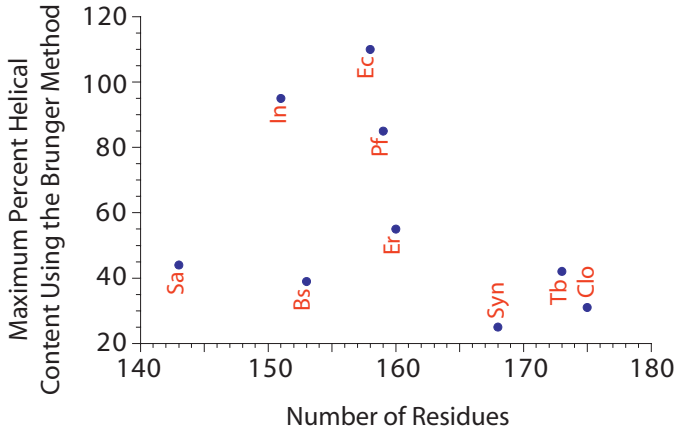

Figure 2.5: Comparison of protein length to the maximal predicted helical content for the various homologues of MscL . No clear trends between protein length and helical content are observerd.

Figure 2.1-A shows the positions of these mutationally sensitive sites mapped onto the Tb-MscL structure. In all cases the alignment we obtain for these residues is the same as others have reported previously. Site directed mutagenesis of Tb-MscL at these positions was performed, converting the wild-type amino acid to a residue shown in *E. coli* to give a GOF phenotype. The resulting mutations were analyzed using plate growth studies and scored using the system described in the Methods section.

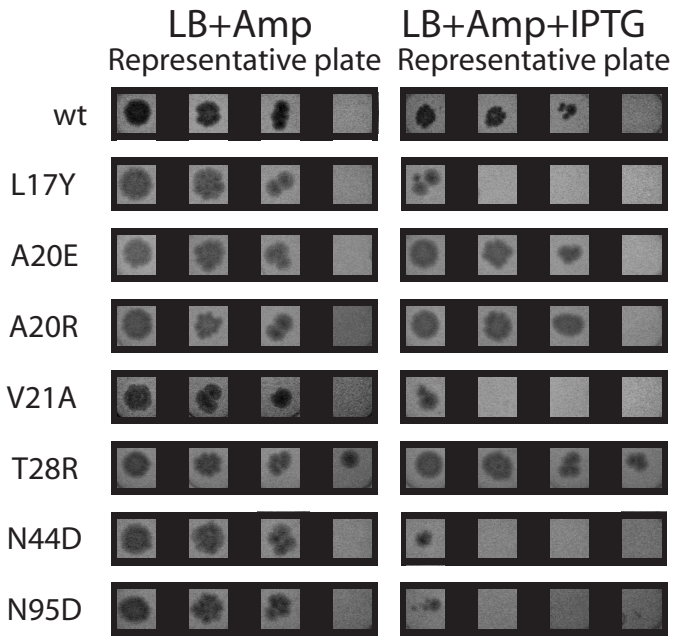

Figure 2.6: Representative plate growth for mutations mapped from *E. coli* MscL to *M. tuberculosis* MscL. The left panel shows the uninduced control and the right panel shows growth in the presence of IPTG. In both panels samples were plated (left to right) from high concentration to low concentration. A GOF phenotype is observed for L17Y, V21A, N44D, and N95D. No difference from wild-type growth is seen for A20E, A20R, and T28R.

Typical plate growth results are shown in Figure 2.6, and all results are gathered in Table 2.2. A GOF phenotype was observed in L17Y, V21A, N44D, and N95D. Unexpectedly, normal growth was observed for A20E, A20R, and T28R, even though the aligned positions, especially A20, were shown to be very sensitive to mutation in Ec-MscL (Batiza and Kung, 2000; Ou et al., 1998; Yoshimura et al., 1999). That mutants displaying normal growth were indeed expressing a MscL channel was verified by SDS-PAGE analysis and Western blotting, which showed levels of protein expression within the variation seen for wild-type Tb-MscL.

Mutant	Number of plates		Average score after 20 h		Average score after 40 h	
	Uninduced	Induced	Uninduced	Induced	Uninduced	Induced
Wild type	51	52	3.38	2.64	3.29	2.75
L17Y	11	11	3.10	0.70	3.19	0.70
A20E	13	13	3.38	3.47	3.38	3.47
A20R	13	13	3.32	3.52	3.32	3.52
V21A	11	11	2.85	1.10	2.85	1.10
T28R	13	13	3.79	3.47	3.79	3.47
N44D	11	11	3.27	0.57	3.27	0.57
N95D	11	11	3.12	0.20	3.20	0.60

Table 2.2: Summarized growth data for GOF mutants mapped from *E. coli* MscL to *M. tuberculosis* MscL.

2.2.4 Verification of the Tb-MscL Structure

Examination of the Tb-MscL structure revealed an intersubunit hydrogen bond, R45•••Q51, located in the loop region of the channel (Figure 2.1-B). Suspecting that such a specific intersubunit contact may be important to function, we mutated this interaction to R45K/Q51E and R45C/Q51C to determine the proximity of these residues under physiological conditions by cross-linking analysis.

The R45K/Q51E mutation was overexpressed and purified from *E. coli*. Cross-linking studies were performed in DDM micelles using EDC or DCC, with or without NHS activators. A typical SDS-PAGE Western blot of cross-linking products is shown in Figure 2.7. Cross-linking is always seen, and in some cases it is quite efficient. After treatment with 10 mM EDC and 10 mM sulfo-NHS, the majority of the observed cross-linked product is tetrameric or pentameric, establishing the high efficiency of this rationally designed cross-linking system.

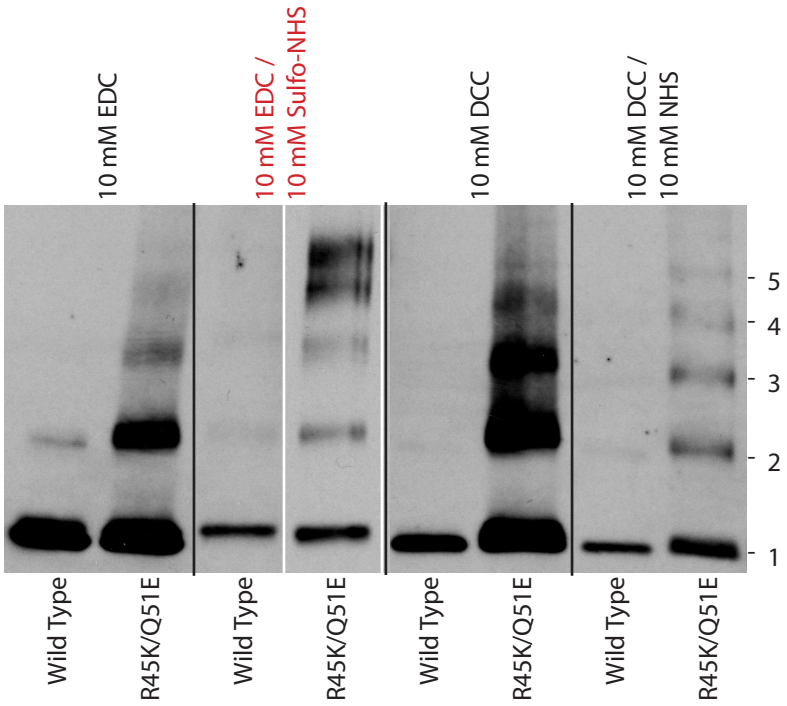

Figure 2.7: Cross-linking of the R45K/Q51E mutant of *M. tuberculosis* MscL. Purified R45K/Q51E *M. tuberculosis* MscL and wild-type protein were cross-linked for 2 hours at 4°C using EDC, DCC, EDC with sulfo-NHS, and DCC with NHS. The reactions were quenched with β-mercaptoethanol, run on a 4-15% SDS-polyacrylamide gel and visualized by Western blotting with 6-His antibody.

Cross-linking of the R45C/Q51C mutant produced similar results to the standard cross-linking of the salt-bridge mutant, but in no instance was highly efficient formation of tetramer and pentamer observed. Disulfide bond formation was induced in the R45C/Q51C mutant by oxidation with copper phenathroline or covalent bond formation was induced using a series of bis-malimide reagents of various tether lengths. The bis-malimide reagents are shown in Figure 2.8, with their associated tether lengths indicated.

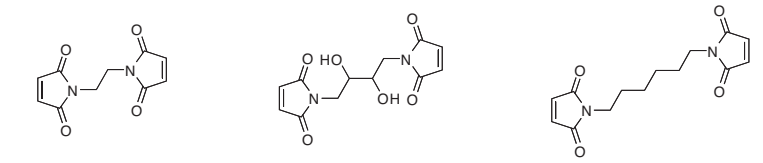

Figure 2.8: Bis-malimide cross-linking reagents with spacer arms of vary lengths.

Typical SDS-PAGE Western blots of the cross-linking reactions are shown in Figure 2.9. Variation in the tether length of the cross-linking reagent from 8.0 Å to 16.1 Å did not affect the cross-linking efficiency of R45C/Q51C Tb-MscL. The variations observed in Figure 2.9 are represntative of variations for a given reaction over several trials.

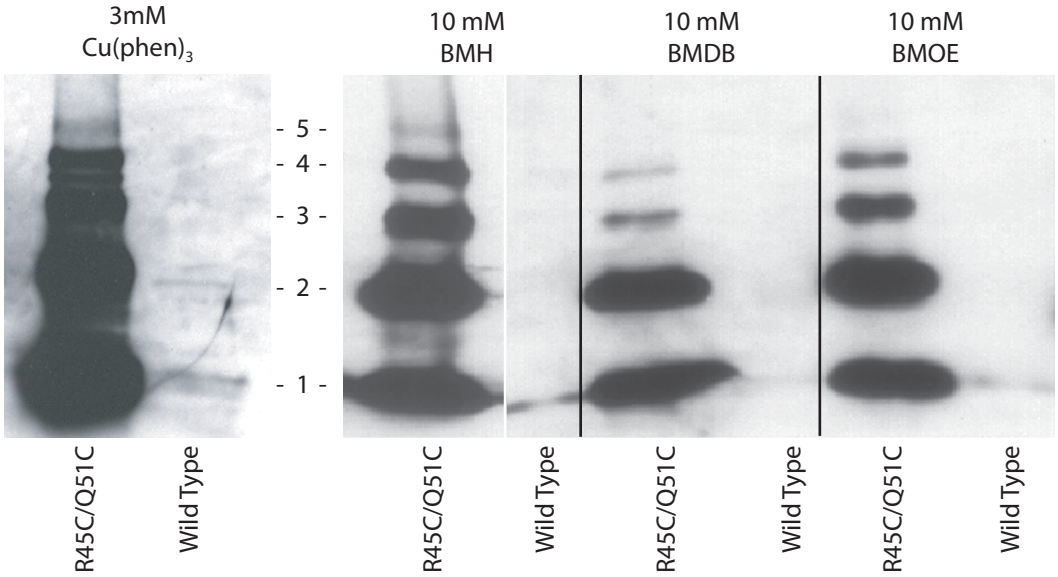

Figure 2.9: Cross-linking of the R45C/Q51C mutant of *M. tuberculosis* MscL. Purified R45C/Q51C *M. tuberculosis* MscL and wild-type protein were cross-linked for 2 hours at 4°C using copper phenanthroline, BMH, BMDB, of BMOE. The reactions were run on a 4-15% SDS-polyacrylamide gel and visualized by Western blotting with 6-His antibody. The copper phenathroline reactions were run in the absence of β-mercaptoethanol.

2.2.5 Functional Characterization of Loop Mutations

Since cross-linking studies confirmed the close proximity of R45 and Q51 under physiological conditions, growth studies were used to assess the effects of mutations at these positions on channel function. The results of growth studies for some single and double mutants at these positions are summarized in Table 2.3, and a representative plate for these mutations is shown in Figure 2.10. All mutations at these positions, with the exception of R45K/Q51K, show a GOF phenotype.

Mutant	Number of plates		Average score after 20 h		Average score after 40 h	
	Uninduced	Induced	Uninduced	Induced	Uninduced	Induced
K45/E51	12	13	3.57	0.00	3.14	0.00
R45K	12	12	3.35	0.00	3.35	0.00
Q51E	12	12	3.07	0.00	3.07	0.00
E45/E51	14	14	3.26	0.64	3.26	0.64
K45/K51	14	14	3.41	3.00	3.62	3.14
C45/C51	12	13	3.65	0.27	3.29	0.43
R45C	12	12	3.59	0.00	3.59	0.00
Q51C	12	12	3.56	0.00	3.56	0.00

Table 2.3: Summarized growth data for mutations of the R45/Q51 hydrogen bond in *M. tuberculosis* MscL.

2.3 Discussion

2.3.1 Sequence Analysis

The MEME sequence analysis has provided insight into the overall similarity of the MscL homologues. Not surprisingly, the homologues are most similar in the transmembrane regions and most divergent in the loop and carboxy terminus regions. The strong similarities in the transmembrane domains are highlighted by the fully conserved groups, II and VIII, and the highly conserved group III. Additionally,

members of the MscL family which lack group III in the first transmembrane region tend to have a similar conserved group IV in this region.

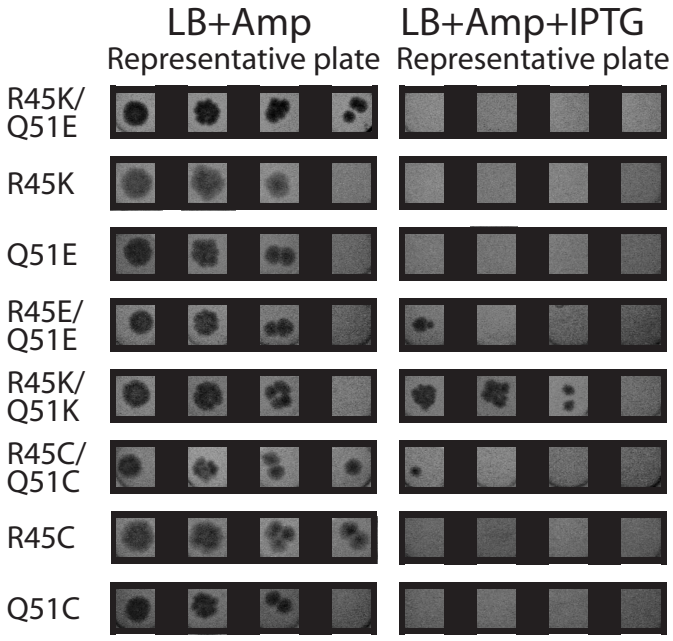

Figure 2.10: Representative plate growth for loop mutations to *M. tuberculosis* MscL. The left panel shows the uninduced control and the right panel shows growth in the presence of IPTG. In both panels samples were plated (left to right) from high concentration to low concentration. A GOF phenotype is observed for R45K/Q51E, R45K, Q51E, R45E/Q51E, R45C/Q51C, R45C, Q51C. No difference from wild-type growth is seen for R45K/Q51K.

The carboxy terminus and loop region are much less conserved. Despite the appearance of three consensus groups in the loop region — V, VI and VII — these groups are clearly not universal. The carboxy terminus is more highly conserved than the loop region, but it is clearly not as well conserved as the transmembrane helices. The carboxy terminus contains two very highly conserved groups — IX and XIII — and the less conserved group XI. Mycobacteria do not contain group IX, but an analogous charged region is evident (group X). Previously it has been shown that a large portion of the carboxy

terminus in Ec-MscL can be deleted without affecting protein function.(Blount et al., 1996b) This is consistent with the lack of sequence conservation in this region.

To further examine the similarities and differences among MscL homologues, a pairwise alignment of the various regions was employed (Figure 2.3). The pairwise alignments showed the same general trends observed with MEME analysis. In general, all regions of the MscL sequence are conserved, however the loop region has pairs of sequences with poor alignment. To some extent the sequence pairs within the loop region can be used to group the homologues into subfamilies. The largest and most obvious subfamily includes *E. coli* MscL and other sequences containing MEME group VI. Another distinctive subfamily includes the Mycobacteria. Thus, by this analysis Ec-MscL and Tb-MscL are in different subfamilies.

2.3.2 Circular Dichroism Studies

As with the sequence analysis, the circular dichroism studies point to two distinct MscL families. However, the families observed by circular dichroism are not the same families that were identified from sequence analysis of putative MscL homologues. In contrast to the results obtained from sequence analysis, Tb-MscL lies in the circular dichroism family with more members and Ec-MscL lies in the circular dichroism family with fewer members.

The helical content of each of the homologues was predicted in an analogous way to that previously used to predict the helical content of Ec-MscL.(Arkin et al., 1998) The two

sequence families show dramatic differences in their predicted helical content, with the first family exhibiting helical contents of 110% to 85% and the second family having a helical content between 55% and 25%.

To determine if the helicity values could be associated with gross differences in secondary structure, the amount of helix in each homologue was predicted using Jpred, a secondary structure prediction program. The predicted helicity values obtained for the MscL homologues using Jpred are quite similar (Table 2.1). It is true that the highest predicted value is for In-MscL, which lies in the Ec-MscL family, and the lowest predicted value is for Clo-MscL, which lies in the Tb-MscL family. However, in general, there is no trend between predicted helical secondary structure and the helical content determined by circular dichroism. In fact, it should be noted that Pf-MscL, which is in the Ec-MscL family, exhibits one of the lowest values for predicted helicity.

The number of amino acids in the homologues examined by circular dichroism varies significantly from 143 to 175 amino acids. However, the predicted helicity from circular dichroism does not correlate with protein length. This is clearly shown in Figure 2.2. The longest and shortest homologues both lie in the Tb-MscL family that displays lower helicity than the Ec-MscL family.

If the Ec-MscL and Tb-MscL families that result from circular dichroism are considered in terms of the sequence analysis, some interesting comparisons result. On the surface, the Tb-MscL family from circular dichroism is composed of seemingly poorly related

sequences. For example, some of the sequences in the Tb-MscL family contain MEME group V and/or MEME group XII, while other members lack these groups. Nonetheless, an interesting similarity between the members of the Tb-MscL family is that all members, other than Er-MscL, lack MEME group VI. In contrast, all of the members of the Ec-MscL family contain MEME group VI, which is located in the loop region. Additionally, Er-MscL has the largest helicity of the Tb-MscL family.

The differences in loop sequence between the two circular dichroism families suggested that it might be possible to identify structural differences from the sequences of this region. To look for structural difference in the loop sequences of the two different families, a FASTA search of the protein structure database (PDB) was performed using the loop regions of the various MscL homologues. This search yielded more helical structures for the Ec-MscL family than for the Tb-MscL family. Sample structures obtained from the search are shown in Figure 2.11. The structural search suggests that members of the Ec-MscL family have dramatically different loop structures than members of the Tb-MscL family. Interestingly these structural differences are reflected in a recent closed state homology model of Ec-MscL (Sukharev et al., 2001a; Sukharev et al., 2001b). Taken together all of the data suggest that the observed differences in the circular dichroism spectra of the MscL homologues may arise from differences in their loop regions.

A

E. coli loop
Initiation factor 4A; 1QVA

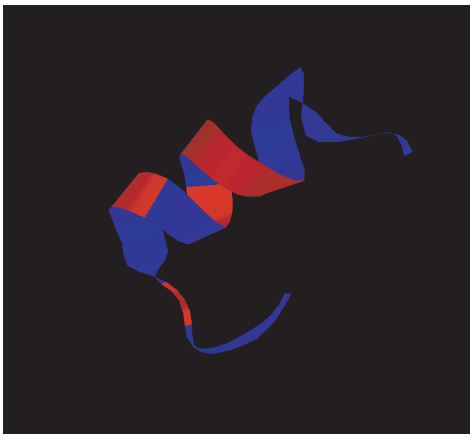

```
GLLIGGIDFKQFAVTLRDAQGDIPAVVMH
   ::: .: . :  :::::
HACIGGTSFVEDAEGLRDAQIVVGTPGRV
```

B

P. fluorescens loop
Flig (Flagellar motor component); 1QC7

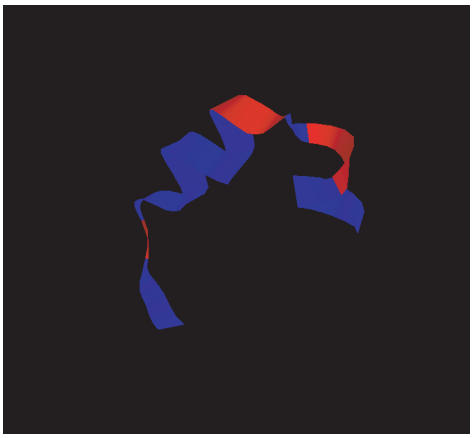

```
GLLIGGVDFSDLAITLKAEGDVPAVVLA
 :..  ::  :::..::. .:
QLVLREVDTRDLALALKGASDELKEKIF
```

C

M. tuberculosis loop
Serratia Metallo Proteinase; 1SMP

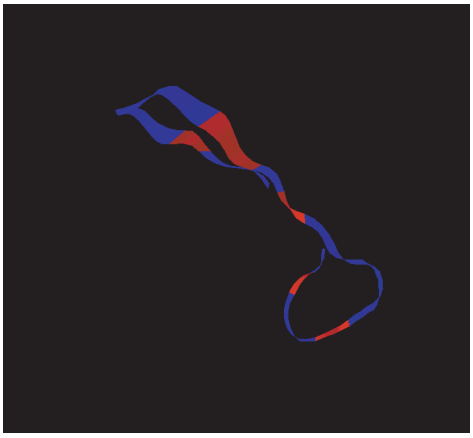

```
NRIGVNAQSDVGILRIGIGGGQTID
  .. ::.:.:  : ..::: :. :
ALLSYNASSNVTDLSVNIGGHQAPD
```

D

C. perfringens loop
C-Src Tyrosine Kinase; 1A1C

```
GSLVGKVDFSNLYINLSGQQFNSLQEAQAAGAATIN
   . :.: ...::. :  ::::::.
HYKIRKLDSGGFYIT-SRTQFNSLQQLVAYYSKHAD
```

Figure 2.11: Sample structures from PDB FASTA searches with MscL loop regions. Only well aligned regions of the loops are shown. Identical and similar residues between the loop and the aligned region of the structure are shown in red.

2.3.3 Mutational Mapping

Previous random mutational analysis of Ec-MscL has focused mainly on the highly conserved transmembrane regions, with only a few mutations in the loop.(Batiza and Kung, 2000; Blount et al., 1997; Blount et al., 1996b; Ou et al., 1998; Yoshimura et al., 1999) For the transmembrane regions, one would expect the sequence homology mapping of the previously obtained GOF *E. coli* mutants onto Tb-MscL to give mutants with a GOF phenotype, due to the high sequence homology in these regions. Note that all alignments, the one reported here and those published previously, agree as to which residues in Tb-MscL correspond to previously studied GOF sites in Ec-MscL.(Batiza et al., 1999; Chang et al., 1998; Oakley et al., 1999; Spencer et al., 1999)

For the majority of mutations studied (L17Y, V21A, N44D, and N95D), the GOF phenotype seen in Ec-MscL is also seen in Tb-MscL (Table 1, Figure 4). Surprisingly, however, mutations at A20 and T28 do not yield a GOF phenotype. The production of Tb-MscL protein for these mutants was confirmed by SDS-PAGE analysis. The lack of GOF phenotype for the A20E and A20R mutants is particularly surprising in light of recent work, which shows that all charged residues at this site give a very severe GOF phenotype in Ec-MscL.(Yoshimura et al., 1999) In fact, only Ala and Gly at these sites produce Ec-MscL with normal function.(Batiza and Kung, 2000)

2.3.4 Tb- MscL Loop Intersubunit Hydrogen Bond

Previous studies of mutations at G46 in Ec-MscL showed the GOF phenotype.(Ou et al., 1998) We have seen similar behavior at the aligned N44 site in Tb-MscL. On examining

the Tb-MscL crystal structure, we observed an intersubunit hydrogen bond involving the adjacent R45 site, with Q51 serving as the partner (Figure 2.1-B). This significant intersubunit interaction suggested an interesting starting point to explore loop function.

Initially, the intersubunit hydrogen bond in the crystal structure was mutated to crosslinkable residues to examine whether these residues are in close proximity under more physiological conditions. The subtle mutation of R45K/Q51E converts the hydrogen bond to a salt bridge. This should still be a favorable intersubunit contact, but the mutant is now susceptible to cross-linking by peptide bond-forming reagents. After overexpression and purification, the protein was exposed to a variety of cross-linking reagents and activators for 2 hours at 4°C. All reagents showed at least a weak pentameric band in the mutant with slight background cross-linking in wild type (Figure 5). The background cross-linking is most likely due to cross-linking in the carboxy terminus of the protein, which contains a number of glutamates, aspartates and lysines.

The most interesting cross-linking results were seen with EDC and Sulfo-NHS. This combination gives mainly pentamer and tetramer for cross-linked products. The strong pentameric band in this designed system provides the best evidence to date that Tb-MscL is pentameric under physiological conditions. Other cross-linking studies typically show progressively weaker band intensities on going from monomer to dimer to trimer, etc., analogous to our results with just EDC and other non-optimal conditions (Figure 2.7) (Blount et al., 1996a; Hase et al., 1997; Sukharev et al., 1999). Such observations always leave open the possibility that a hexamer band is present, but is too weak to be seen as the

intensity progressively falls off with higher oligomerization. Under some conditions, a weak band assigned to hexamer has been seen. However, with the designed double mutant under appropriate conditions (EDC/Sulfo-NHS), very strong tetramer and pentamer bands are seen, but no hexamer band is visible. This provides compelling evidence that no significant fraction of Tb-MscL is present in hexameric (or higher oligomerization) states when reconstituted in DDM micelles.

Cross-linking studies using R45C/Q51C Tb-MscL did not produce the quantitative results observed with R45K/Q51E Tb-MscL. However, high molecular weight bands were observed upon cross-linking, either by oxidation of the free thiols to disulfides or by reaction with bis-malimide reagents (Figure 2.9). Interestingly, when R45C/Q51C Tb-MscL was cross-linked using bis-malimide reagents of varying tether lengths, no distance dependence was observed for cross-linking efficiency. This observation is consistent with the nearly quantitative cross-linking observed for R45K/Q51E Tb-MscL and implies that these side chains are in close proximity.

2.3.5 Functional Studies of the Tb-MscL Loop

After confirming that the residues R45 and Q51 were within interaction distance, we performed growth studies on both single and double mutants to examine channel function. All single mutants (R45K, Q51E, R45C, and Q51C) and all double mutants (R45K/Q51E, R45E/Q51E, and R45C/Q51C) except R45K/Q51K displayed a GOF phenotype (Table 2.3). The lack of a GOF phenotype for the R45K/Q51K mutant is surprising and merits further study. Nevertheless, this region appears to be quite

mutationally sensitive. Note that the R45K mutation is subtle, suggesting that the loop plays a central role in channel gating. Recently it has been shown that proteolytic cleavage of the loop significantly alters channel gating (Ajouz et al., 2000), supporting our view of a critical functional role for this region.

2.4 Conclusions and Future Directions

These studies suggest that although *M. tuberculosis* and *E. coli* MscL are similar, there are important differences. Thus, caution should be exercised when employing the Tb-MscL crystal structure to explain functional results for Ec-MscL. Most strikingly, mutations at A20 in Tb-MscL do not exhibit a GOF phenotype, despite the extreme sensitivity of the aligned G22 in *E. coli*. Additionally, the loop region of Tb-MscL appears highly sensitive to mutations, suggesting that the loop region in general and the R45•••Q51 intersubunit hydrogen bond in particular, merit further investigation.

Using the alignment of Figure 2, there is no obvious Ec-MscL analogue to the R45•••Q51 hydrogen bond seen in Tb-MscL. Technically, the alignment is L47/D53 (Ec-MscL numbering), which is not a favorable interaction. There is no cationic or hydrogen bond donating residue near L47 that could pair with D53. However, residues on either side of D53 are hydrophobic, suggesting that perhaps the ion pair of Tb-MscL is replaced by a hydrophobic contact such as L47/I52 or L47/F54 in Ec-MscL. It would be interesting to investigate this possibility.

The differences between the families of MscL homologues obtained from sequence analysis and those obtained from circular dichroism analysis are quite intriguing. In order to get a clear understanding of observed families, experimental examination of additional MscL homologues is needed. Preliminary comparison of the circular dichrosim data with reported electrophysiology data (Moe et al., 1998) did not yield an explanation of the circular dichrosim family classification. However more detailed electrophysiology may allow for the rationalization of these families.

Significant differences clearly exist between Tb-MscL and Ec-MscL, although further comparisons, such as those described in Chapter 5, are still needed to fully understand the variations in these channels. Structural difference between Tb-MscL and Ec-MscL may exist in the loop as well as other regions of the protein. Designed cross-linking reactions provide clear evidence for the validity of the Tb-MscL crystal structure, and the high homology exhibited between the transmemberane domains of Tb-MscL and Ec-MscL suggest the Ec-MscL has a similar overall architecture.

2.5 Materials and Methods

2.5.1 Sequence Analysis

Multiple sequence alignments were obtained using AMPS (Alignment of Multiple Sequences)(Barton, 1990; Barton and Sternberg, 1987) and consensus group analysis was performed using MEME (Multiple EM for Motif Elicitation).(Bailey and Elkan, 1994; Bailey and Gribskov, 1998) The alignment was broken into regions–extracellular loop, carboxy terminus, and transmembrane regions one and two–using the helix definitions of

Chang *et al*.(Chang et al., 1998) The extracellular loop is defined as the region between the first and second transmembrane domains, and the carboxy terminus is the region from the end of the second transmembrane domain to the end of the carboxy helix. Pairwise alignments of the various regions were performed using AMPS, and scores for each pair were summarized as contour plots. Scores reflect the alignment of sequence A to sequence B relative to a shuffled sequence B and are therefore corrected for length. Scores above 5 indicate very good alignment between two protein sequences, scores between 2 and 5 indicate moderate alignment, and scores below 2 indicate poor alignment.

2.5.2 Constructs, Strains, and Cell Growth

All mutations were generated from a pET 19b (Novagen) construct containing the *M. tuberculosis* MscL open reading frame (Chang et al., 1998) using the QuikChange Method (Stratagene). Mutations were confirmed by enzymatic digest and sequencing. Expression and growth studies were carried out in BL21(DE3) *E. coli* using an MscL knockout mutant (Chang et al., 1998). All bacterial growth was done in the presence of 100 μg/mL ampicillin.

Growth studies were carried out as previously described (Yoshimura et al., 1999). Cells were grown in LB media to an OD_{600} of approximately 0.6 and diluted to an OD_{600} of 0.2±0.02. The cells were further diluted to 10^{-3}, 10^{-4}, 10^{-5}, and 10^{-6} and spotted (5 μL) onto 12-well LB plates in the presence or absence of 1 mM IPTG. Plates were imaged and scored after 20 and 40 hours. A scoring system was developed, in which the score

for a given growth plate was incremented by one for each concentration in which growth was observed (maximum score of 4). A minimum of 11 replications from four separate dilutions were obtained for each mutant.

Protein expression was performed by growing cells to the midpoint of log phase and inducing with 0.1% IPTG and 1% lactose. Following induction, cells were grown for an additional 2 hours, harvested, and solubilized in 1% DDM, 10 mM TRIS, and 10 mM NaCl. Protein was purified on a nickel-chelation column (Qiagen) in the presence of 0.05% DDM. The resulting proteins were verified by MALDI-TOF mass spectral analysis.

2.5.3 Circular Dichroism Studies

Circular dichrosim studies were preformed on an Aviv 42a DS circular dichroism spectrometer using a strain-free circular cuvette with a pathlength of 0.1 cm. Spectra were collected between 260 nm and 185 nm and averaged over three scans. All data was collected at room temperature. Concentrations for conversion to molar elipticy units were obtained using the BioRad DC compatible protein concentration kit or the Peirce BCA protein concentration kit.

2.5.4 Cross-linking Studies

Wild-type or R45K/Q51E protein solubilized in DDM micelles was diluted to a concentration of approximately 25 μg/mL and cross-linked at 4^{o}C for 2 hours using 10 mM EDC, 10 mM DCC, 10 mM EDC/10 mM Sulfo-NHS, or 10 mM DCC/10 mM NHS.

All cross-linking reactions were quenched with SDS-PAGE loading buffer containing β-mercaptoethanol. Reaction products were run on 4-15% gradient polyacrylamide gels and visualized by Western blotting with either a 6-His Antibody (Amersham) or INDIA HisProbe-HRP (Pierce). Cysteine cross-linking reactions were performed and assayed in a similar manner on wild type and R45C/Q51C Tb-MscL. Thioethers were formed with bis-maleimide reagents (Pierce), or disulfide bonds were formed with 3 mM copper phenanthroline. For the copper phenanthroline studies β-mercaptoethanol was omitted from the loading buffer.

2.6 Literature Cited

Ajouz, B., Berrier, C., Besnard, M., Martinac, B., and Ghazi, A. (2000). Contributions of the different extramembranous domains of the mechanosensitive ion channel MscL to its response to membrane tension. Journal of Biological Chemistry *275*, 1015-1022.

Arkin, I. T., Sukharev, S. I., Blount, P., Kung, C., and Brunger, A. T. (1998). Helicity, membrane incorporation, orientation and thermal stability of the large conductance mechanosensitive ion channel from *E-coli*. Biochim Biophys Acta-Biomembr *1369*, 131-140.

Bailey, T. L., and Elkan, C. (1994). Fitting a mixture model by expectation maximization to discover motifs in bioploymers. Paper presented at: Second International Conference on Intelligent Systems for Molecular Biology (Menlo Park, California, AAAI Press).

Bailey, T. L., and Gribskov, M. (1998). Combining evidence using p-values: application to sequence homology searches. Bioinformatics *14*, 48-54.

Barton, G. J. (1990). Protein Multiple Sequence Alignment and Flexible Pattern-Matching. Methods in Enzymology *183*, 403-428.

Barton, G. J., and Sternberg, M. J. E. (1987). A Strategy For the Rapid Multiple Alignment of Protein Sequences - Confidence Levels From Tertiary Structure Comparisons. Journal of Molecular Biology *198*, 327-337.

Batiza, A. F., and Kung, C. (2000). The hydrophobicity of residue 22 is not sufficient for G22X MscL functioning upon hypotonic shock. Biophysical Journal *78*, 473A-473A.

Batiza, A. F., Rayment, I., and Kung, C. (1999). Channel gate! Tension, leak and disclosure. Structure, Folding, and Design *7*, R99-R103.

Blount, P., and Moe, P. C. (1999). Bacterial mechanosensitive channels: integrating physiology, structure and function. Trends in Microbiology *7*, 420-424.

Blount, P., Ou, X., Hoffman, R. J., and Kung, C. (1998). Characterization of randomly generated mutants of MscL, a mechanosensitive channel in bacteria, identifies a functional region of the protein. Biophysical Journal *74*, A324-A324.

Blount, P., Schroeder, M. J., and Kung, C. (1997). Mutations in a bacterial mechanosensitive channel change the cellular response to osmotic stress. Journal of Biological Chemistry *272*, 32150-32157.

Blount, P., Sukharev, S. I., Moe, P. C., Schroeder, M. J., Guy, H. R., and Kung, C. (1996a). Membrane topology and multimeric structure of a mechanosensitive channel protein of *Escherichia coli*. Embo J *15*, 4798-4805.

Blount, P., Sukharev, S. I., Schroeder, M. J., Nagle, S. K., and Kung, C. (1996b). Single residue substitutions that change the gating properties of a mechanosensitive channel in *Escherichia coli*. Proceedings of the National Academy of Sciences of the United States of America *93*, 11652-11657.

Chang, G., Spencer, R. H., Lee, A. T., Barclay, M. T., and Rees, D. C. (1998). Structure of the MscL homolog from *Mycobacterium tuberculosis*: A gated mechanosensitive ion channel. Science *282*, 2220-2226.

Cuff, J. A., and Barton, G. J. (1999). Application of enhanced multiple sequence alignment profiles to improve secondary structure prediction. Proteins *40*, 502-511.

Hase, C. C., Minchin, R. F., Kloda, A., and Martinac, B. (1997). Cross-linking studies and membrane localization and assembly of radiolabelled large mechanosensitive ion channel (MscL) of *Escherichia coli*. Biochemical and Biophysical Research Communications *232*, 777-782.

Liu, W., Deitmer, J. W., and Martinac, B. (1999). Glycine G14, the amino acid essential for electromechanical coupling in gating the MscL of *E. coli* by mechanical force. Biophysical Journal *76*, A203-A203.

Moe, P. C., Blount, P., and Kung, C. (1998). Functional and structural conservation in the mechanosensitive channel MscL implicates elements crucial for mechanosensation. Molecular Microbiology *28*, 583-592.

Moe, P. C., Levin, G., and Blount, P. (2000). Correlating a protein structure with function of a bacterial mechanosensitive channel. Journal of Biological Chemistry *275*, 31121-31127.

Oakley, A. J., Martinac, B., and Wilce, M. C. J. (1999). Structure and function of the bacterial mechanosensitive channel of large conductance. Protein Science *8*, 1915-1921.

Ou, X. R., Blount, P., Hoffman, R. J., and Kung, C. (1998). One face of a transmembrane helix is crucial in mechanosensitive channel gating. Proceedings of the National Academy of Science of the United States of America *95*, 11471-11475.

Rees, D. C., Chang, G., and Spencer, R. H. (2000). Crystallographic analyses of ion channels: Lessons and challenges. Journal of Biological Chemistry *275*, 713-716.

Shapovalov, G., and Lester, H. A. (2000). Unpublished Results.

Spencer, R. H., Chang, G., and Rees, D. C. (1999). 'Feeling the pressure': structural insights into a gated mechanosensitive channel. Current Opinions in Structural Bioliogy *9*, 448-454.

Sukharev, S., Betanzos, M., Chiang, C. S., and Guy, H. R. (2001a). The gating mechanism of the large mechanosensitive channel MscL. Nature *409*, 720-724.

Sukharev, S., Durell, S. R., and Guy, H. R. (2001b). Structural models of the MscL gating mechanism. Biophysical Journal *81*, 917-936.

Sukharev, S., Schroeder, M. J., and McCaslin, D. R. (1999). Re-examining the multimeric structure of the large conductance bacterial mechanosensitive channel, MscL. Biophysical Journal *76*, A138-A138.

Yoshimura, K., Batiza, A., Schroeder, M., Blount, P., and Kung, C. (1999). Hydrophilicity of a single residue within MscL correlates with increased channel mechanosensitivity. Biophysical Journal *77*, 1960-1972.